

SAGA-HE-202
 YAMAGATA-HEP-03-30
 September, 2003

Maximum Entropy Method Approach to θ Term

Masahiro Imachi^{†*†}),
 Yasuhiko Shinno^{◇**}) and Hiroshi Yoneyama^{◇***})

Department of Physics, Yamagata University, Yamagata 990-8560, Japan[†]

Department of Physics, Saga University, Saga 840-8502, Japan[◇]

Abstract

In Monte Carlo simulations of lattice field theory with a θ term, one confronts the complex weight problem, or the sign problem. This is circumvented by performing the Fourier transform of the topological charge distribution $P(Q)$. This procedure, however, still causes the flattening phenomenon of the free energy, which prevents one from studying the phase structure. In order to work at this issue, we apply the maximum entropy method (MEM) to the Gaussian $P(Q)$, which serves as a good laboratory to test whether the MEM works for the θ term. We study the case with the flattening as well as the one without the flattening. For the latter case, the results of the MEM agree with the Fourier transform, and for the former the flattening is much improved.

^{*}) E-mail: imachi@sci.kj.yamagata-u.ac.jp

^{**}) E-mail: shinno@dirac.phys.saga-u.ac.jp

^{***}) E-mail: yoneyama@cc.saga-u.ac.jp

§1. Introduction

It is expected that a θ term could affect the dynamics at low energy and vacuum structure of QCD, but it is known from experimental evidences that the value of θ is very suppressed in Nature. From the theoretical point of view, the reason is not so clear yet. Hence it is important to study the properties of QCD with the θ term to clarify the structure of QCD vacuum.¹⁾ For theories with the θ term, it is pointed out that rich phase structures could be realized in θ space. For example, the phase structure of the $Z(N)$ gauge model was investigated by using free energy arguments, and it was found that oblique confinement phases could occur.²⁾ In CP^{N-1} models, which have several dynamical properties in common with QCD, it was shown that a first-order phase transition exists at $\theta = \pi$.^{3),4),5)}

Although the numerical simulation is one of the most effective tools to study non-perturbative properties of field theories, the introduction of the θ term makes the Boltzmann weight complex. This makes it difficult to perform Monte Carlo (MC) simulations on the euclidean lattice. This is the complex action problem or the sign problem. In order to circumvent this problem, the following way is conventionally employed;^{6),7)} the partition function $\mathcal{Z}(\theta)$ can be obtained by Fourier-transforming the topological charge distribution $P(Q)$, which is calculated with real positive Boltzmann weight.

$$\mathcal{Z}(\theta) = \frac{\int [d\bar{z}dz] e^{-S+i\theta\hat{Q}(\bar{z},z)}}{\int [d\bar{z}dz] e^{-S}} \equiv \sum_Q e^{i\theta Q} P(Q), \quad (1.1)$$

where

$$P(Q) \equiv \frac{\int [d\bar{z}dz]_Q e^{-S}}{\int d\bar{z}dz e^{-S}}. \quad (1.2)$$

The measure $[d\bar{z}dz]_Q$ in Eq. (1.2) represents that the integral is restricted to configurations of the field z with the topological charge Q , and S denotes an action.

In the study of CP^{N-1} models, it is known that this algorithm works well for small lattice volume V and in the strong coupling region.^{6),4),8),9)} As volume increases or in the weak coupling region, however, this strategy suffers from the sign problem for $\theta \simeq \pi$ again. The errors of $P(Q)$ mask the true values of $\mathcal{Z}(\theta)$ in the vicinity of $\theta = \pi$, and may give a fictitious signal of a phase transition.¹⁰⁾ This is called flattening, because the free energy becomes almost flat for θ larger than a certain value. This could be remedied by reducing the errors of $P(Q)$. It is, however, hopeless because the statistics to beat the errors become exponentially increasing with V . Recently, an alternative method has been proposed to circumvent the sign problem.^{11),12)}

Our motivation in the present paper is to reconsider the issue from the point of view of the maximum entropy method (MEM).^{13),14),15),16)} The MEM is well known as a powerful

tool for so-called ill-posed problems, where the number of parameters to be determined is much larger than the number of data. It is applied to a wide range of fields such as radio astrophysics and condensed matter physics. Recently, spectral functions in lattice field theory have been widely studied by use of the MEM.^{16),17),18),19)} In the present paper, we are interested in whether the MEM could work in the study of the θ term and to what extent one can improve the flattening phenomenon of the free energy.

The MEM is based upon the Bayes' theorem. It derives the most probable parameters by utilizing data sets and our knowledge about these parameters in terms of the probability. The probability distribution, which is called posterior probability, is given by the product of the likelihood function and the prior probability. The latter is represented by the Shannon-Jaynes entropy, which plays an important role to guarantee the uniqueness of the solution, and the former is given by χ^2 . It should be noted that artificial assumptions are not needed during the calculations since exploring a unique solution is performed according to the probability theory. Our task is to explore the image such that the posterior probability is maximized. In practice, however, it is difficult to find a unique solution in huge configuration space of the image. In order to find it effectively, we employ the singular value decomposition (SVD).

The flattening of the free energy is an inherent phenomenon in the Fourier transformation procedure. It is quite independent of what models one deals with. We choose the Gaussian $P(Q)$, which is widely realized in the cases such as the strong coupling region of the CP^{N-1} model and the 2-d $U(1)$ gauge model. Since the Gaussian $P(Q)$ is analytically Fourier-transformed to $\mathcal{Z}(\theta)$, it is a good laboratory to investigate whether the MEM would work. For the analysis, we use mock data by adding noise to $P(Q)$ in the case with the flattening as well as without the flattening.

Our conclusion is summarized as follows.

1. In the case without the flattening, the results of the MEM agree with those of the Fourier transformation and thus reproduce the exact results.
2. In the case with the flattening, we find a good deal of improvement with the flattening phenomenon.

This paper is organized as follows. In the following section, we overview the origin of the flattening. In section 3 we summarize the procedure for the analysis of the MEM. The results obtained by use of the MEM are presented in section 4. Summary is given in section 5.

§2. Sign problem and flattening behavior of free energy

In this section, we briefly review the flattening phenomenon of the free energy density. It is observed when one employs the algorithm in which $\mathcal{Z}(\theta)$ is calculated through the Fourier transform. In order to obtain $\mathcal{Z}(\theta)$, we must calculate $P(Q)$ with high precision. Although $P(Q)$ is calculated over a wide range of digits by use of the set method,²⁰⁾ the errors of $P(Q)$ disturb the behavior of $\mathcal{Z}(\theta)$ through the Fourier transform. Its effect becomes serious at large θ region. Here, we use the Gaussian $P(Q)$ for the discussion. The Gaussian $P(Q)$ is not just a toy model but is realized in a variety of models such as the 2-d U(1) gauge model and in the strong coupling limit of CP^{N-1} models.

We parameterize the Gaussian $P(Q)$ by

$$P(Q) = A \exp\left[-\frac{c}{V}Q^2\right], \quad (2\cdot1)$$

where, in the case of the 2-d U(1) gauge model, c is a constant depending on the inverse coupling constant β and V the lattice volume. Hereafter V is regarded as a parameter, and varied in the analysis. The constant A is fixed so that $\sum_Q P(Q) = 1$. The distribution $P(Q)$ is analytically transformed by use of the Poisson's sum formula to the partition function

$$\mathcal{Z}_{\text{pois}}(\theta) = A \sqrt{\frac{\pi V}{c}} \sum_{n=-\infty}^{\infty} \exp\left[-\frac{V}{4c}(\theta - 2\pi n)^2\right]. \quad (2\cdot2)$$

For preparing the mock data, we add noise with the variance of $\delta \times P(Q)$ to the Gaussian $P(Q)$. In the analysis, we set up data sets with various values of δ and study the effects of δ .

Fig.1 displays the Gaussian $P(Q)$ for various lattice volumes V . The parameter c is fixed at $c = 7.42$. Corresponding free energy density, $f(\theta) = -\frac{1}{V} \log \mathcal{Z}(\theta)$, calculated by Eq. (1·1), are shown in Fig.2. All $f(\theta)$ in Fig. 2 falls on a universal line for $\theta \lesssim 2.3$. For $\theta \gtrsim 2.3$, finite size effects are clearly observed; as volume increases, $f(\theta)$ increases until $V \lesssim 20$, but for $V = 30$ and $V = 50$ the Fourier transformation does not work. At $V = 30$ $\mathcal{Z}(\theta)$ becomes negative for certain values of θ , and at $V = 50$, $f(\theta)$ becomes almost flat for $\theta \gtrsim 2.3$. The latter behavior gives a fictitious signal of a first-order phase transition at $\theta \approx 2.3$. The mechanism of this flattening^{8),5)} is briefly summarized as follows.

The distribution $P(Q)$ obtained from MC simulations can be decomposed into two parts, a true value and an error of $P(Q)$.

$$P(Q) = \tilde{P}(Q) + \Delta P(Q), \quad (2\cdot3)$$

where $P(Q)$, $\tilde{P}(Q)$ and $\Delta P(Q)$ denote the MC data, the true value and the error, respectively. In order to calculate $P(Q)$ efficiently, which ranges many orders, the set method and

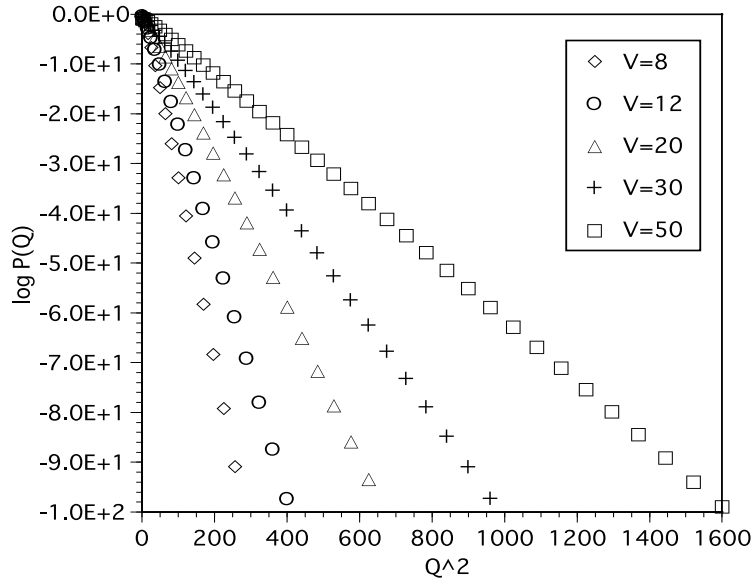


Fig. 1. Gaussian topological charge distribution for various lattice volumes. The parameter δ is chosen to be 1/400.

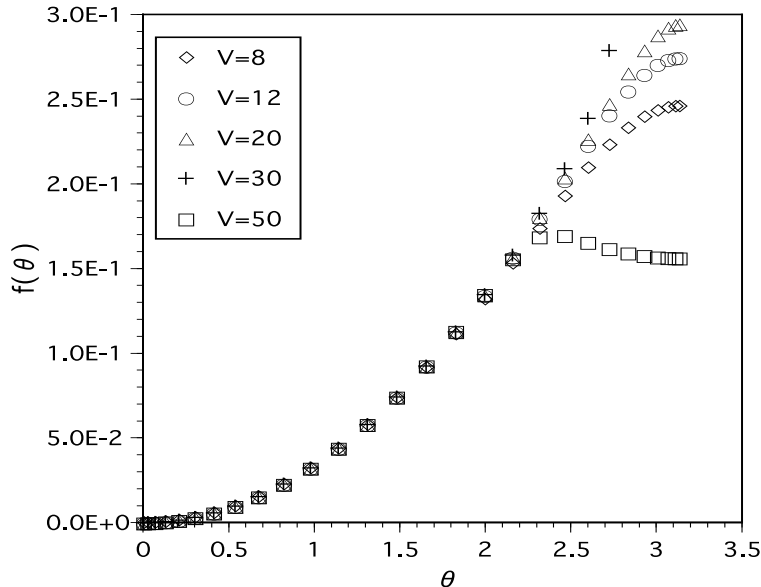


Fig. 2. Free energy density $f(\theta)$ for various lattice volumes. $f(\theta)$ is calculated numerically by Fourier-transforming the Gaussian topological charge distribution.

the trial function method are conventionally used. In the set method, the range of Q is divided into several sets, each of which consists of a couple of bins. At each set, the topological charge of the configurations is calculated in order to construct the histogram. The trial function method makes the distribution of the histogram almost flat. This is useful for

reducing the errors of $P(Q)$. Accordingly the errors are computed as⁴⁾

$$\Delta P(Q) \sim \delta P(Q) \times P(Q),$$

where $\delta P(Q)$ is almost independent of Q . Since $P(Q)$ is a rapidly decreasing function, so is the statistical error $\Delta P(Q)$. Thus the dominant contribution of $\Delta P(Q)$ comes from that at $Q = 0$, and the partition function $\mathcal{Z}(\theta)$ suffers from the error $\Delta P(0) \approx \delta P(0)P(0) \approx \delta P(0)$. The free energy density for the MC data is approximately given by

$$\begin{aligned} f(\theta) &= -\frac{1}{V} \log \mathcal{Z}(\theta) \approx -\frac{1}{V} \log \left\{ \sum_Q \tilde{P}(Q) e^{i\theta Q} + \delta P(0) \right\} \\ &= -\frac{1}{V} \log \left\{ e^{-V\tilde{f}(\theta)} + \delta P(0) \right\}, \end{aligned} \quad (2.4)$$

where $\tilde{f}(\theta)$ is the true free energy density. The value of $e^{-V\tilde{f}(\theta)}$ decreases rapidly as the volume V and/or θ increase (see Fig. 2), and then the magnitude of $e^{-V\tilde{f}(\theta)}$ becomes the order of $\delta P(0)$ at $\theta \simeq \theta_f$. Therefore $f(\theta)$ cannot be calculated precisely but $f(\theta) \simeq \text{const}$ for $\theta \gtrsim \theta_f$. This is the reason for the flattening behavior of $V = 50$ at $\theta \gtrsim \theta_f \simeq 2.3$ as shown in Fig. 2. A drastic reduction of $\Delta P(Q)$ is necessary in order to estimate property $f(\theta)$ for $\theta \gtrsim \theta_f$. In the case of a large volume, however, this is hopeless because exponentially increasing statistics are needed. So we do need some other way to calculate $f(\theta)$.

§3. MEM

In this section we explain briefly the concept of the MEM and the necessary procedures for the analysis to make this paper self-contained and to fix the notations.

3.1. MEM based on Bayes' theorem

In an experiment or a numerical simulation, data are always noisy and the number of the data set is finite. It is in principle impossible to reconstruct the true image from these data sets. Hence it is reasonable to search for the most probable image in terms of the probability. From the Bayes' theorem, the probability that the image \mathbf{f} occurs under a given data set $\{\mathbf{D}\}$ is represented by

$$\text{prob}(\mathbf{f}|\mathbf{D}) = \frac{\text{prob}(\mathbf{D}|\mathbf{f})\text{prob}(\mathbf{f})}{\text{prob}(\mathbf{D})}, \quad (3.1)$$

where $\text{prob}(A)$ is the probability that an event A occurs and $\text{prob}(A|B)$ is the conditional probability that A occurs under a condition B . Moreover, one can add to Eq. (3.1) 'prior information' I about the image \mathbf{f} . The information I contains the one obtained from theoretical restrictions as well as knowledge based on the previous experiments. Eq. (3.1) becomes

$$\text{prob}(\mathbf{f}|\mathbf{D}, I) = \frac{\text{prob}(\mathbf{D}|\mathbf{f}, I)\text{prob}(\mathbf{f}|I)}{\text{prob}(\mathbf{D}|I)}, \quad (3.2)$$

where $\text{prob}(A, B)$ is the joint probability that events A and B occur simultaneously. The probability $\text{prob}(\mathbf{f}|\mathbf{D}, I)$ is called posterior probability. When the probability $\text{prob}(\mathbf{D}|\mathbf{f}, I)$ is considered as a function of \mathbf{f} for fixed data, it is equivalent to the likelihood function, which expresses how data points vary around the 'true value' corresponding to the true image \mathbf{f} . The probability $\text{prob}(\mathbf{f}|I)$ is called prior probability and represents our state of knowledge about the image \mathbf{f} before the experiment is done. The most probable image satisfies a condition

$$\frac{\delta \text{prob}(\mathbf{f}|\mathbf{D}, I)}{\delta \mathbf{f}} = 0. \quad (3.3)$$

Recently, the MEM is applied to hadronic spectral functions in lattice QCD.^{16),17)} In the analysis of the spectral function $A(\omega)$, the correlation function $D(\tau)$ is given as

$$D(\tau) = \int_0^\infty d\omega K(\tau, \omega) A(\omega), \quad (3.4)$$

where $K(\tau, \omega)$ denotes the kernel of the Laplace transform. In lattice theories, the number of the data points is, at most, the order of $10 \sim 10^2$ due to finite volume, while the number of the degrees of freedom to describe the continuous function $A(\omega)$ ranges $\mathcal{O}(10^2) \sim \mathcal{O}(10^3)$.

Turning to theories with the θ term, the object we have to deal with is

$$P(Q) = \int_{-\pi}^{\pi} d\theta \frac{e^{-i\theta Q}}{2\pi} \mathcal{Z}(\theta). \quad (3.5)$$

Compared to Eq. (3.4), one can see a resemblance as follows

$$\{P(Q) \leftrightarrow D(\tau), e^{-i\theta Q}/2\pi \leftrightarrow K(\tau, \omega), \mathcal{Z}(\theta) \leftrightarrow A(\omega)\}, \quad (3.6)$$

namely, the continuous function $\mathcal{Z}(\theta)$ must be reconstructed from the finite number of data for $P(Q)$, i.e., an ill-posed problem. What we would like to do in the present paper is then to rely on the MEM according to

$$\text{prob}(\mathcal{Z}(\theta)|P(Q), I) = \text{prob}(\mathcal{Z}(\theta)|I) \frac{\text{prob}(P(Q)|\mathcal{Z}(\theta), I)}{\text{prob}(P(Q)|I)}. \quad (3.7)$$

The likelihood function $\text{prob}(P(Q)|\mathcal{Z}(\theta), I)$ is given by

$$\text{prob}(P(Q)|\mathcal{Z}(\theta), I) = \frac{e^{-\frac{1}{2}\chi^2}}{X_L}, \quad (3.8)$$

where X_L is a normalization constant, and χ^2 is represented by

$$\chi^2 \equiv \sum_{Q, Q'} (P^{(\mathcal{Z})}(Q) - \bar{P}(Q)) C_{Q, Q'}^{-1} (P^{(\mathcal{Z})}(Q') - \bar{P}(Q')) \quad (3.9)$$

in our case, where $P^{(\mathcal{Z})}(Q)$ is constructed from $\mathcal{Z}(\theta)$ through Eq. (3.5). And $\bar{P}(Q)$ denotes the average of a data set $\{P(Q)\}$;

$$\bar{P}(Q) = \frac{1}{N_d} \sum_{l=1}^{N_d} P^{(l)}(Q), \quad (3.10)$$

where N_d represents the number of the data set. The matrix C^{-1} is an inverse covariance made up by the data set $\{P(Q)\}$.

The prior probability $\text{prob}(\mathcal{Z}(\theta)|I)$ is represented in terms of the entropy S

$$\text{prob}(\mathcal{Z}(\theta)|I, \alpha) = \frac{e^{\alpha S}}{X_S(\alpha)}, \quad (3.11)$$

where α is a real positive parameter and $X_S(\alpha)$ denotes an α -dependent normalization constant. The choice of the entropy S is somewhat flexible. Conventionally, the Shannon-Jaynes entropy is employed;

$$S = \int_{-\pi}^{\pi} d\theta \left[\mathcal{Z}(\theta) - m(\theta) - \mathcal{Z}(\theta) \log \frac{\mathcal{Z}(\theta)}{m(\theta)} \right], \quad (3.12)$$

where $m(\theta)$ is called default model. The default model $m(\theta)$ must be taken so as to be consistent with prior knowledge.

Therefore the posterior probability $\text{prob}(\mathcal{Z}(\theta)|P(Q), I, \alpha, m)$ is rewritten as

$$\text{prob}(\mathcal{Z}(\theta)|P(Q), I, \alpha, m) = \frac{e^{-\frac{1}{2}\chi^2 + \alpha S}}{X_L X_S(\alpha)}, \quad (3.13)$$

where it is explicitly shown that α and m are regarded as new prior knowledge in $\text{prob}(\mathcal{Z}(\theta)|P(Q), I, \alpha, m)$.

The information I restricts regions to be searched in image space and helps us with exploring a solution effectively; we impose a criterion

$$\mathcal{Z}(\theta) > 0 \quad (3.14)$$

so that $\text{prob}(\mathcal{Z}(\theta) \leq 0|I, m) = 0$.

In order to obtain the best image of $\mathcal{Z}(\theta)$, one must find the solution such that a function

$$W \equiv -\frac{1}{2}\chi^2 + \alpha S \quad (3.15)$$

is maximized for a given α ;

$$\frac{\delta}{\delta \mathcal{Z}(\theta)} \left(-\frac{1}{2}\chi^2 + \alpha S \right) \Big|_{\mathcal{Z}=\mathcal{Z}^{(\alpha)}} = 0. \quad (3.16)$$

The parameter α plays a role of the relative weight between S and $\frac{1}{2}\chi^2$. For $\alpha = 0$, the solution of Eq. (3.16) corresponds to the maximal likelihood, while for $\alpha \gg 1$ $\mathcal{Z}(\theta) = m(\theta)$ is realized as a solution. Therefore the choice of $m(\theta)$ needs some care.

3.2. procedure for analysis

In the numerical analysis, the continuous function $\mathcal{Z}(\theta)$ is discretized; $\mathcal{Z}(\theta) \rightarrow \mathcal{Z}(\theta_n) \equiv \mathcal{Z}_n$. The integral over θ in Eq. (3.5) is converted to the finite summation over θ ;

$$P_j = \left\{ \begin{array}{ll} \sum_{n=1}^{N_\theta} \frac{1}{2\pi} \mathcal{Z}_n & (j=1) \\ \sum_{n=1}^{N_\theta} \frac{\cos \theta_n j}{\pi} \mathcal{Z}_n & (\text{otherwise}) \end{array} \right\} \equiv \sum_{n=1}^{N_\theta} K_{jn} \mathcal{Z}_n \quad (3.17)$$

where $j = 1, 2, \dots, N_q$. Note that $N_q < N_\theta$. P_j denotes $P(Q)$ at $Q = j - 1$. Here we used the fact that $P(Q)$ and $\mathcal{Z}(\theta)$ are even functions of Q and θ , respectively. Eq. (3.12) is also discretized as

$$S = \sum_{n=1}^{N_\theta} \left[\mathcal{Z}_n - m_n - \mathcal{Z}_n \log \frac{\mathcal{Z}_n}{m_n} \right], \quad (3.18)$$

where $m(\theta_n) \equiv m_n$.

We take the following procedure for the analysis.^{13),16)}

1. Maximizing W for a fixed α :

In order to find the image that maximizes W in functional space of \mathcal{Z}_n for a given α , we calculate Eq. (3.16). This yields

$$-\alpha \log \frac{\mathcal{Z}_n}{m_n} = \sum_{i,j=1}^{N_q} K_{in} C_{ij}^{-1} \delta P_j \quad (n = 1, 2, \dots, N_\theta), \quad (3.19)$$

where C_{ij} is the covariance matrix in Eq. (3.9), and

$$\delta P_j \equiv P_j^{(\mathcal{Z})} - \bar{P}_j. \quad (3.20)$$

Solving \mathcal{Z}_n is non-trivial, because N_θ is $\mathcal{O}(10^1 \sim 10^2)$ and $N_q \sim \mathcal{O}(10^0)$ in our case. It is convenient to use the SVD and the Newton method. The detail is discussed in Appendix A. The solution to Eq. (3.19) is called $\mathcal{Z}_n^{(\alpha)}$.

2. Averaging $\mathcal{Z}_n^{(\alpha)}$:

Since α is an artificial parameter, the finally obtained image must have no α -dependence. The α -independent final image can be calculated by averaging the image $\mathcal{Z}_n^{(\alpha)}$ according to the probability. The expectation value of \mathcal{Z}_n is given as

$$\hat{\mathcal{Z}}_n = \int [d\mathcal{Z}] \mathcal{Z}_n \text{prob}(\mathcal{Z}_n | P(Q), I, m), \quad (3.21)$$

where the measure $[d\mathcal{Z}] \equiv \prod_n d\mathcal{Z}_n / \sqrt{\mathcal{Z}_n}$ is used.¹³⁾ By using the law of the total probability and the conditional probability, we obtain

$$\begin{aligned}\hat{\mathcal{Z}}_n &= \int [d\mathcal{Z}] \mathcal{Z}_n \int d\alpha \text{prob}(\mathcal{Z}_n | \alpha, P(Q), I, m) \text{prob}(\alpha | P(Q), I, m) \\ &\simeq \int d\alpha \text{prob}(\alpha | P(Q), I, m) \mathcal{Z}_n^{(\alpha)}.\end{aligned}\quad (3\cdot22)$$

Further use of the total probability, the conditional probability and the Bayes' theorem to $\text{prob}(\alpha | P(Q), I, m)$ yields

$$\hat{\mathcal{Z}}_n = \frac{1}{X_W} \int d\alpha \mathcal{Z}_n^{(\alpha)} \exp \left\{ \Lambda(\alpha) + W(\mathcal{Z}^{(\alpha)}) \right\}, \quad (3\cdot23)$$

where X_W is a normalization constant, and $\Lambda(\alpha) \equiv \frac{1}{2} \sum_k \log \frac{\alpha}{\alpha + \lambda_k}$. Here the values λ_k 's are eigenvalues of the real symmetric matrix in θ space;

$$\frac{1}{2} \sqrt{\mathcal{Z}_m} \frac{\partial^2 \chi^2}{\partial \mathcal{Z}_m \partial \mathcal{Z}_n} \sqrt{\mathcal{Z}_n} \Big|_{\mathcal{Z}=\mathcal{Z}^{(\alpha)}}. \quad (3\cdot24)$$

In deriving Eq. (3\cdot23), we assumed that the probability $\text{prob}(\mathcal{Z}_n | \alpha, P(Q), I, m)$ has a sharp peak around $\mathcal{Z}_n^{(\alpha)}$, and $W(\mathcal{Z}^{(\alpha)})$ denotes the value of W for $\mathcal{Z}_n = \mathcal{Z}_n^{(\alpha)}$. The derivation of Eq. (3\cdot23) is done in Appendix B.

In averaging over α , we determine a range of α so that $\text{prob}(\alpha | P(Q), I, m) \geq \frac{1}{10} \times \text{prob}(\hat{\alpha} | P(Q), I, m)$ holds, where $\text{prob}(\alpha | P(Q), I, m)$ is maximized at $\alpha = \hat{\alpha}$. The normalization constant is given such that

$$\int_{\alpha_{min}}^{\alpha_{max}} d\alpha \text{prob}(\alpha | P(Q), I, m) = 1. \quad (3\cdot25)$$

3. Error estimation:

One of the advantages of the MEM is to be able to estimate the errors of constructed images. Since the errors of \mathcal{Z}_n among different points could be correlated, the error estimation should be performed over some range Θ in θ space. The range Θ is determined systematically by analyzing the Hessian matrix in θ space.

$$H_{m,n} \equiv \frac{\partial^2 W}{\partial \mathcal{Z}_m \partial \mathcal{Z}_n} \Big|_{\mathcal{Z}=\mathcal{Z}^{(\alpha)}}. \quad (3\cdot26)$$

The uncertainty of the final output image $\hat{\mathcal{Z}}_n$ is calculated as follows.¹⁶⁾

$$\langle (\delta \hat{\mathcal{Z}}_n)^2 \rangle \equiv \int d\alpha \langle (\delta \mathcal{Z}_n^{(\alpha)})^2 \rangle \text{prob}(\alpha | P(Q), I, m), \quad (3\cdot27)$$

where

$$\begin{aligned}\langle(\delta\mathcal{Z}^{(\alpha)})^2\rangle &\equiv \frac{\int[d\mathcal{Z}]\int_{\Theta}d\theta_nd\theta_{n'}\delta\mathcal{Z}_n\delta\mathcal{Z}_{n'}\text{prob}(\mathcal{Z}_m|P(Q),I,m,\alpha)}{\int[d\mathcal{Z}]\int_{\Theta}d\theta_nd\theta_{n'}\text{prob}(\mathcal{Z}_m|P(Q),I,m,\alpha)} \\ &\simeq -\frac{1}{\int_{\Theta}d\theta_nd\theta_{n'}}\int_{\Theta}d\theta_nd\theta_{n'}\left(\frac{\partial^2W}{\partial\mathcal{Z}_n\partial\mathcal{Z}_{n'}}\Big|_{\mathcal{Z}=\mathcal{Z}^{(\alpha)}}\right)^{-1}.\end{aligned}\quad (3.28)$$

See Appendix B for the detail.

In a sequence of procedure described in this section, the uniqueness of the final image is guaranteed for $\alpha \neq 0$. It requires the conditions that the image $\mathcal{Z}^{(\alpha)}(\theta)$ is positive definite and that the kernel $(K^t)_{nj}$ is real. These are satisfied as shown in Appendix C.

§4. Results

In this section, we present the results of the MEM analysis of the data for $P(Q)$. Preparing data for the analysis, we add to $P(Q)$ Gaussian noise generated with the variance $\delta \times P(Q)$ for each value of Q . This is based on the observations in the procedure which was employed to calculate $P(Q)$ in the simulations of models such as the CP^{N-1} model.⁴⁾ This turns out to yield errors with almost constant portion of $P(Q)$ for each Q as shown in Eq. (2.4). The parameter δ is varied from $1/10$ to $1/600$ and we present the results with $\delta = 1/400$. A set of data consists of $P(Q)$ with the errors from $Q = 0$ to $Q = N_q - 1$. By setting up such N_d sets of data, we calculate the covariance matrices in Eq.(3.9) through the jackknife method. We have checked whether the outcome is stable by varying the value of N_d for a range of $10 \leq N_d \leq 60$ and have found that this is the case for $30 \lesssim N_d$. We present here the results for $N_d = 30$.

As to the default model $m(\theta)$ in Eq.(3.12), we study various cases: (i) $m(\theta) = \text{const}$, (ii) $m(\theta) = (\sin(\theta/2)/(\theta/2))^V \equiv m_{\text{strg}}(\theta)$, (iii) $m(\theta) = \exp(-\frac{\ln 10}{\pi^2}\gamma\theta^2)$. In the case of (i), we studied several values such as $m(\theta) = 0.1, 0.3$ and 1.0 . We show the results of $m(\theta) = 1.0$ as a typical case. The case (ii) is the strong coupling limit of the CP^{N-1} model. The case (iii) is the Gaussian. The parameter γ is varied in the analysis.

The number of degrees of freedom in θ space, N_{θ} , is larger than that of the topological charge N_q . The number N_q is chosen so as to satisfy $P(Q) \geq 10^{-30}$ in the non-flattening case and $P(Q) \geq 10^{-11}$ in the flattening case, and varies 3 to 8 depending on V . The covariance matrix appears in Eq.(3.9);

$$C_{Q,Q'} = \frac{1}{N_d(N_d-1)} \sum_{l=1}^{N_d} (P^{(l)}(Q) - \bar{P}(Q))(P^{(l)}(Q') - \bar{P}(Q')), \quad (4.1)$$

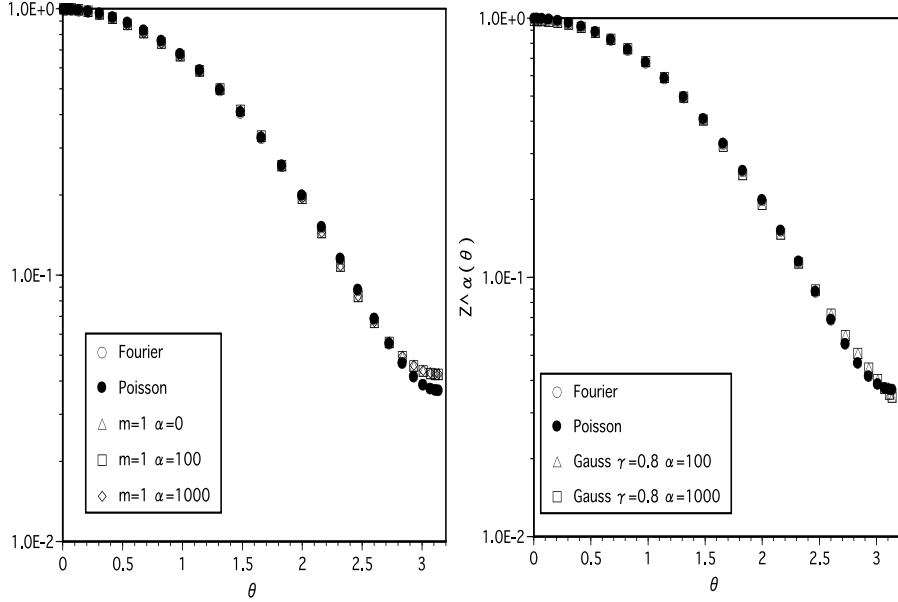


Fig. 3. $\mathcal{Z}^{(\alpha)}(\theta)$ for the data without the flattening. $V = 12$. The default model $m(\theta)$ is chosen to be 1.0 and the Gaussian with $\gamma = 0.8$.

where $P^{(l)}(Q)$ denotes the l -th data of the topological charge distribution and $\bar{P}(Q)$ is the average Eq.(3.10). The inverse covariance matrix is calculated with precision that the product of the covariance matrix and its inverse has off-diagonal elements at most $\mathcal{O}(10^{-27})$.

The other degrees of freedom N_θ is varied from 10 to 100, and it is found that the results are stable for $25 \lesssim N_\theta$. In the following results, N_θ is set to be 28. Note that in order to reproduce $\mathcal{Z}(\theta)$ which ranges many orders, the analysis must be performed with quadruple precision.

4.1. MEM analysis of the data without the flattening

Before discussing to what extent the flattening behavior of the free energy is remedied, we discuss the case without the flattening. It is non-trivial whether the MEM can work for our issue.

The data of $V \leq 20$ are used for the analysis, where no flattening behavior is observed (see Fig. 2). For the present we concentrate on the data of $V = 12$. For this value of V , two types of default models are employed; the constant default model, $m(\theta) = 1.0$, and the Gaussian one with $\gamma = 0.4 \sim 1.0$.

The maximal image $\mathcal{Z}^{(\alpha)}(\theta)$ of $\mathcal{Z}(\theta)$ for a given α is calculated by Eq. (3.16). Fig.3 displays $\mathcal{Z}^{(\alpha)}(\theta)$ for various α ($0 \leq \alpha \leq 1000$) in the cases of $m(\theta) = 1.0$ and the Gaussian with $\gamma = 0.8$. It is found that the α -dependence of $\mathcal{Z}^{(\alpha)}(\theta)$ is hardly seen and that the images approximately agree with the result of the Fourier transform and thus with the exact

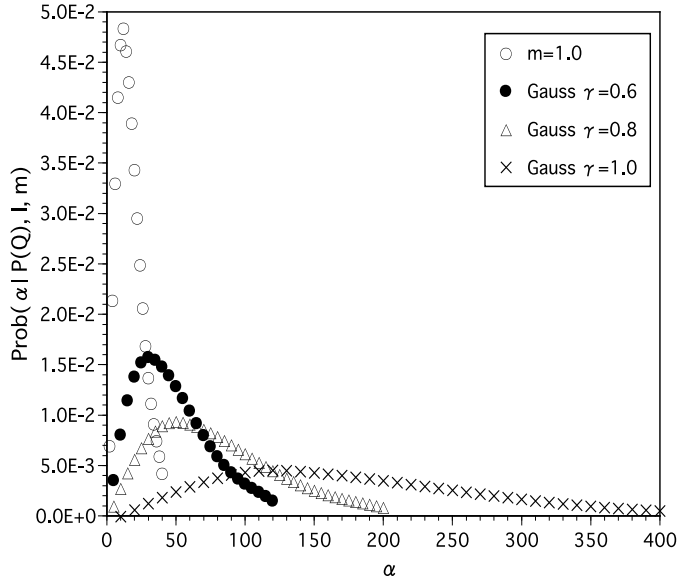


Fig. 4. $\text{prob}(\alpha|P(Q), I, m)$ for the data without the flattening. $V = 12$. The default model is chosen to be $m(\theta) = 1.0$ and the Gaussian with $\gamma = 0.6, 0.8$ and 1.0 .

partition function $\mathcal{Z}_{\text{pois}}(\theta)$.

In order to investigate which $\mathcal{Z}^{(\alpha)}(\theta)$ is the most probable, we calculate the posterior probability $\text{prob}(\alpha|P(Q), I, m)$ in Eq. (3.23). The data of $\text{prob}(\alpha|P(Q), I, m)$ are fitted by smooth functions and are normalized such that Eq. (3.25) holds. The results are plotted in Fig.4. For both of the cases, $\text{prob}(\alpha|P(Q), I, m)$ has a peak at a small value of α ; for $m(\theta) = 1.0$, the peak is located at $\alpha \simeq 12.0$, while it is located at $\alpha \simeq 30.0$ ($\gamma = 0.6$), $\alpha \simeq 50.0$ ($\gamma = 0.8$) and $\alpha \simeq 120.0$ ($\gamma = 1.0$) in the Gaussian case. Since $\mathcal{Z}^{(\alpha)}(\theta)$'s do not have the α -dependence in the region around the peak, the integrals to obtain the averaged image $\hat{\mathcal{Z}}(\theta)$ in Eq. (3.23) are trivially performed and $\hat{\mathcal{Z}}(\theta)$'s are approximately in agreement with the exact one.

For $V = 8$ and 20 , similar analyses are performed. We find that the characteristics of $\mathcal{Z}^{(\alpha)}(\theta)$ and $\text{prob}(\alpha|P(Q), I, m)$ stated above, namely, $\mathcal{Z}^{(\alpha)}(\theta)$ is hardly dependent on α for not so large values ($\lesssim 1000$) and $\text{prob}(\alpha|P(Q), I, m)$ has a peak at a small value of α , also hold for $V = 8$ and 20 . Therefore we obtain the same consequences with $\hat{\mathcal{Z}}(\theta)$. In more general, in the non-flattening case where the Fourier transform works well, the fact that the image obtained by the MEM agrees with the result of the Fourier transform is understood by having a close look at the equations used in the SVD. This is discussed analytically in Appendix D.

The detailed procedure for estimating the errors $\delta\hat{\mathcal{Z}}(\theta)$ is discussed in the next subsection and its results are shown in the end.

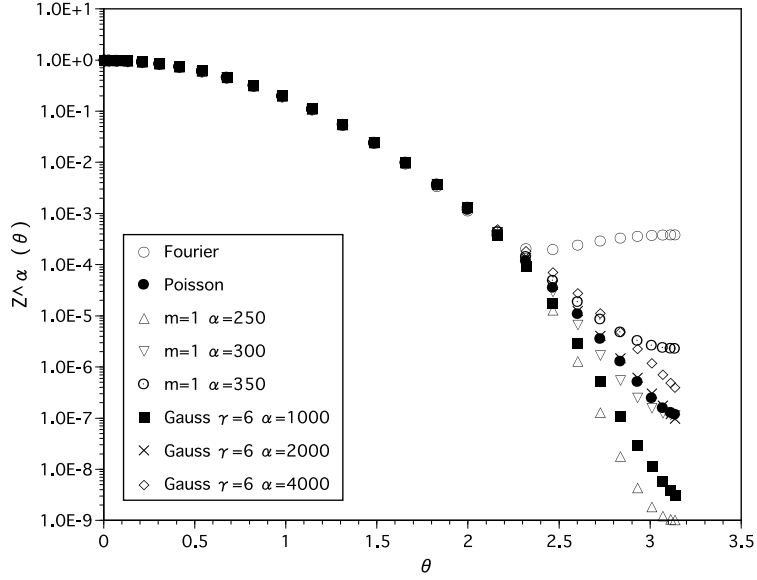


Fig. 5. $\mathcal{Z}^{(\alpha)}(\theta)$ for the data with the flattening. The default model $m(\theta)$ is chosen to be 1.0 and the Gaussian with $\gamma = 6$. Comparing with the result of the Fourier transform (circle), the result of the MEM for certain value of α , $\alpha \approx 300$ for $m(\theta) = 1.0$ and $\alpha \approx 2000$ for the Gaussian, reproduces approximately well that of the exact partition function Eq.(2.2) (solid circle).

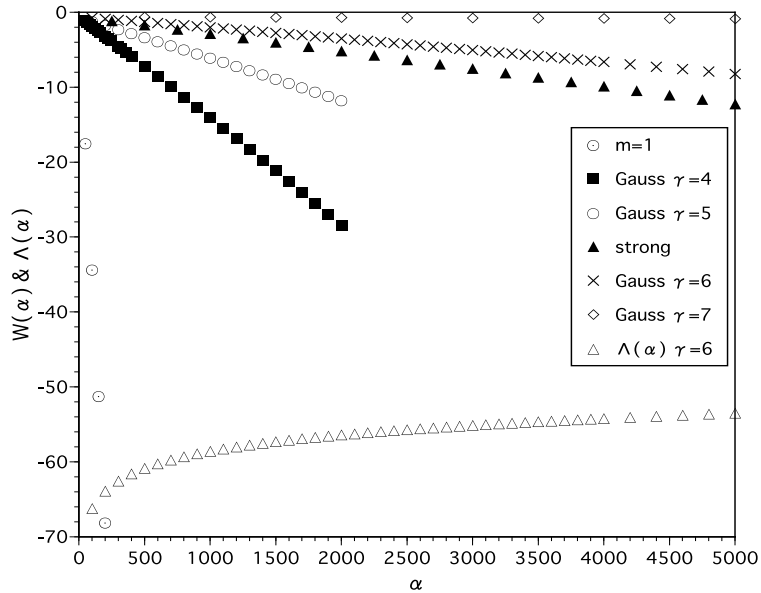


Fig. 6. $W(\mathcal{Z}^{(\alpha)})$ for various $m(\theta)$ and for $V = 50$. $W(\mathcal{Z}^{(\alpha)})$ is shown for $m_{\text{strg}}(\theta)$ and for the Gaussian default with $\gamma = 4, 5, 6$ and 7. $\Lambda(\alpha)$ appearing in Eq. (3.23) is also plotted in the same scale. Since $\Lambda(\alpha)$ does not depend so much on $m(\theta)$, $\Lambda(\alpha)$ for the Gaussian default with $\gamma = 6$ is displayed as a reference.

4.2. MEM analysis of the data with the flattening

Let us turn to the case with the flattening. Unlike the case without the flattening, the images of $\mathcal{Z}(\theta)$ show quite different behaviors from those of the Fourier transform. We fix volume to be $V = 50$ for a while. Fig.5 displays $\mathcal{Z}^{(\alpha)}(\theta)$ calculated by $m(\theta) = 1.0$ and the Gaussian default with $\gamma = 6$, which are images determined by maximizing Eq.(3.15) for each α . For each of the defaults, maximal images are free from the flattening, and at least for a certain value of α , there exists $\mathcal{Z}^{(\alpha)}(\theta)$ which is in reasonable agreement with the exact one $\mathcal{Z}_{\text{pois}}(\theta)$. This also holds for $m(\theta) = \text{Gaussian}$ case with $\gamma = 4, 5$ and 7 , although the value of α giving an agreement with $\mathcal{Z}_{\text{pois}}(\theta)$ varies depending on that of γ . In the case of $m_{\text{strg}}(\theta)$, however, we find no agreement even when α is varied from $\mathcal{O}(1)$ to $\mathcal{O}(10^6)$.

The posterior probability $\text{prob}(\alpha|P(Q), I, m)$ is calculated by Eq. (B.4) appearing in Eq. (3.23). Fig. 6 displays the behavior of $W(\mathcal{Z}^{(\alpha)})$ and $\Lambda(\alpha)$ for various $m(\theta)$. We find that as α increases, $W(\mathcal{Z}^{(\alpha)})$ decreases almost linearly, depending strongly on $m(\theta)$, while $\Lambda(\alpha)$ increases showing rather little α -dependence. The sum of $W(\mathcal{Z}^{(\alpha)})$ and $\Lambda(\alpha)$ gives $\text{prob}(\alpha|P(Q), I, m)$, and a balance between the two determines the location of a peak of $\text{prob}(\alpha|P(Q), I, m)$ if it exists. This is shown in Fig.7.

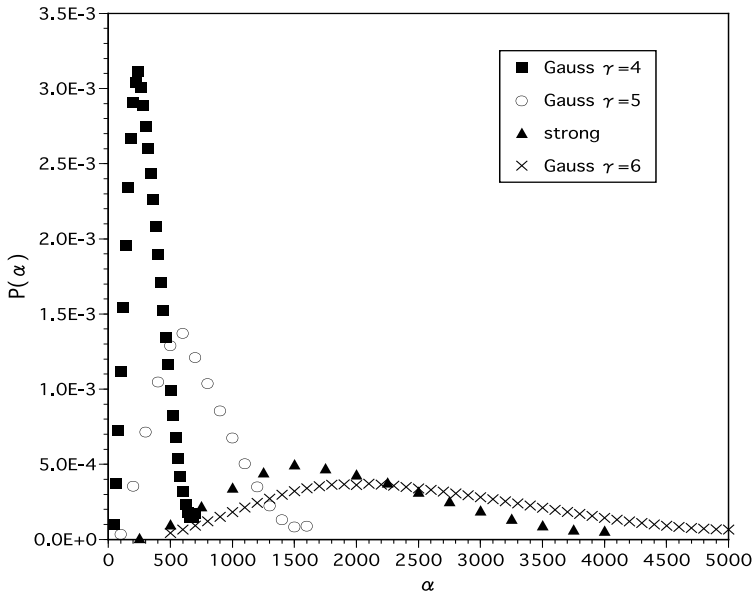


Fig. 7. $\text{prob}(\alpha|P(Q), I, m)$ for various $m(\theta)$. V is fixed to be 50.

The averaged image $\hat{\mathcal{Z}}(\theta)$ is calculated by Eq.(3.23). Upon integrating over α , the data of $\text{prob}(\alpha|P(Q), I, m)$ are fitted by a smooth function and is normalized. Fig.8 displays $\hat{\mathcal{Z}}(\theta)$ for various $m(\theta)$. In the case of the Gaussian $m(\theta)$, the parameter γ is varied from 4 to 8. We find a reasonably good agreement between $\gamma = 5$ and 6 . This is due to the fact that for these cases the best value of α in $\mathcal{Z}^{(\alpha)}(\theta)$ is approximately equal to the location of

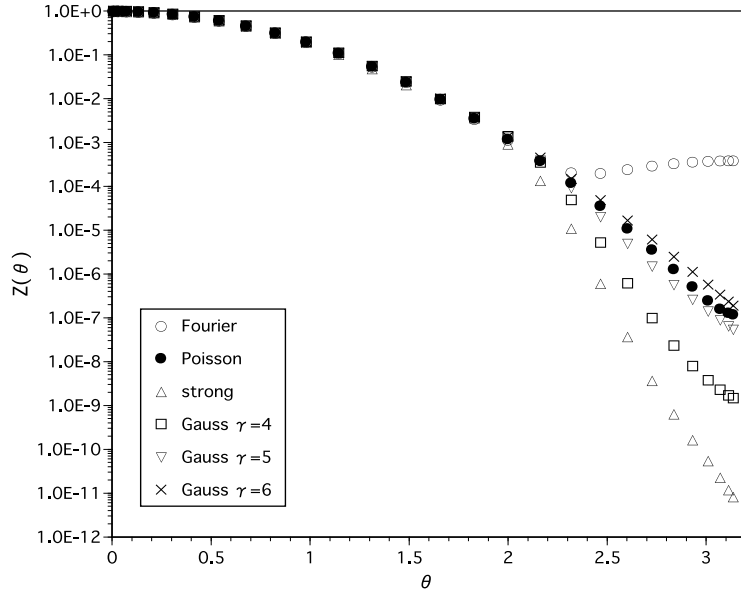


Fig. 8. Averaged partition function $\hat{Z}(\theta)$ for various $m(\theta)$. Volume is fixed to be 50. The result of the Fourier transform is also included. Those for the Gaussian default with $\gamma = 5$ and 6 reasonably agree with the exact result $Z_{\text{pois}}(\theta)$. The result for $m_{\text{strg}}(\theta)$ shows a large deviation from $Z_{\text{pois}}(\theta)$.

the peak of $\text{prob}(\alpha|P(Q), I, m)$; for $\gamma = 6$ the both values agree (≈ 2000), and for $\gamma = 5$ they are slightly different (≈ 1000 and $\hat{\alpha} \approx 650$). In other words, these images could occur with high probability. In the case of $m(\theta) = 1.0$ case, although the best image was in good

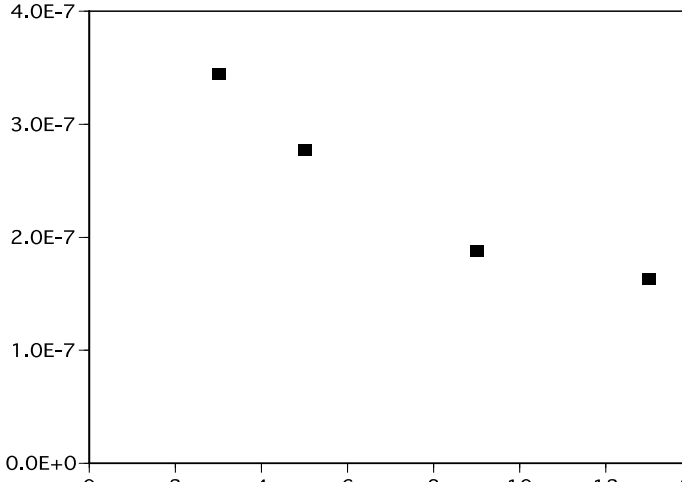


Fig. 9. Errors estimated at $\theta = 3.07$ by varying the block size for $\gamma = 15.5$ and $V = 50$. See text for the detail.

agreement with $Z_{\text{pois}}(\theta)$ for $\alpha = 300$ as shown in Fig.5, the peak of $\text{prob}(\alpha|P(Q), I)$ is located at $\alpha < 40.0$. This large difference in α leads to a large deviation of $\hat{Z}(\theta)$ from the correct one $Z_{\text{pois}}(\theta)$. Similarly, for $m_{\text{strg}}(\theta)$, the image $Z^{(\alpha)}(\theta)$ in agreement with $Z_{\text{pois}}(\theta)$ occur in a

very low probability and consequently $\hat{\mathcal{Z}}(\theta)$ deviates largely from $\mathcal{Z}_{\text{pois}}(\theta)$. This is obvious, because $\mathcal{Z}^{(\alpha)}(\theta)$ never agrees with $\mathcal{Z}_{\text{pois}}(\theta)$ for $\alpha = \mathcal{O}(1)$ to $\mathcal{O}(10^6)$. Note that the errors are not included in the figure.

One of the advantages of the MEM analysis is to be able to estimate the errors according to the probability that the images realize. In fact, the obtained images are meaningless unless their errors are evaluated. We use the formula Eq.(3.28) for the error estimates. The error $\delta\hat{\mathcal{Z}}(\theta_n)$ of $\hat{\mathcal{Z}}(\theta_n)$ is estimated by integrating θ in Eq.(3.28) over the range $\Theta = \theta_{n-b/2}$ and $\theta_{n+b/2}$, where θ_m is the abscissa in the Gauss-Legendre N -point ($N=100$) quadrature formula for the range $0 \leq \theta \leq \pi$. Fig.9 displays a typical behavior of the error as a function of block size at $\theta = 3.07$ for $m(\theta)=\text{Gaussian}$ with $\gamma = 5.5$, where the block size is defined by $b + 1$. Upon estimating the errors, we compare the magnitude of the errors of $\hat{\mathcal{Z}}(\theta)$

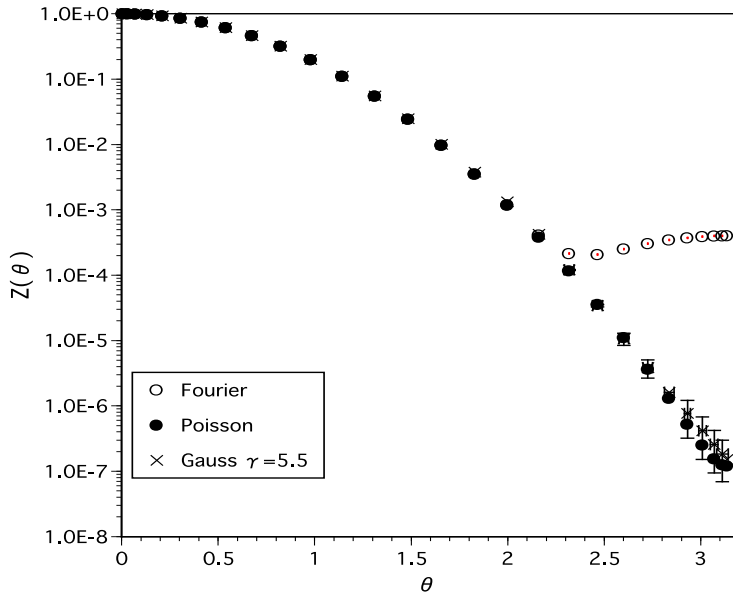


Fig. 10. $\hat{\mathcal{Z}}(\theta)$ (cross) with the error bars for the Gaussian default with $\gamma = 5.5$. $V = 50$. Compared to the result of the Fourier transform (circle), a remarkable improvement is clearly seen.

for $\gamma = 5, 5.5$ and 6 . It turns out that those for $\gamma = 5.5$ are the smallest among them. Fig.10 shows the partition function with the estimated errors for the Gaussian default with $\gamma = 5.5$. The result does not show the flattening but is consistent with $\mathcal{Z}_{\text{pois}}(\theta)$. For the other default models, $m(\theta) = 1.0$ and $m_{\text{strg}}(\theta)$, it is found that the errors are too large to obtain reasonable images $\hat{\mathcal{Z}}(\theta)$.

We apply the same procedure to the data for the other volumes. Table I gives $\hat{\mathcal{Z}}(\theta)$ and $\delta\hat{\mathcal{Z}}(\theta)$ at $\theta = 2.30$ and 3.07 for various volumes and default models. Each of the two θ 's is chosen as a reference, where the latter is closed to π and the former is near θ_f . The default models listed in Table give almost minimal errors among the defaults we have investigated

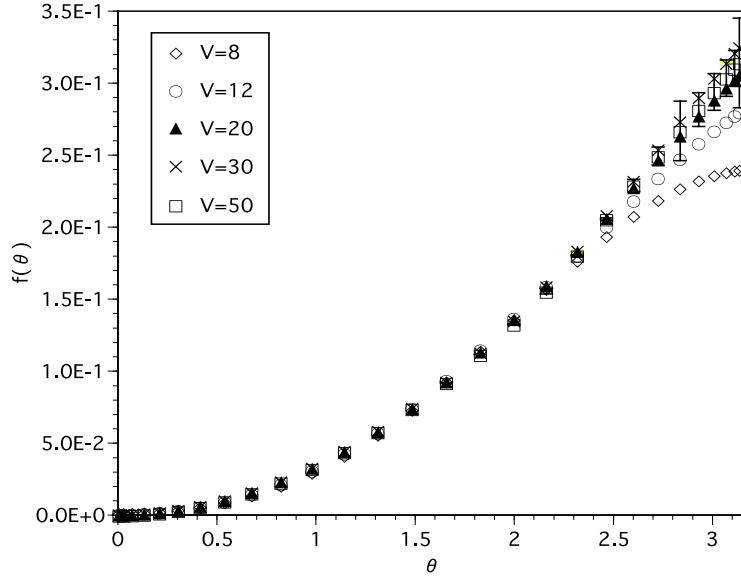


Fig. 11. Free energy density $f(\theta)$ calculated from $\hat{\mathcal{Z}}(\theta)$ for various volumes. See Fig.2 for a comparison.

Table I. $\hat{\mathcal{Z}}(\theta)$ at $\theta = 2.30$ and $\theta = 3.07$ for various volumes V . The default model is chosen to be the Gaussian with γ . The exact values $\mathcal{Z}_{\text{pois}}(\theta)$ are also listed.

V	γ (Gaussian default)	$\mathcal{Z}_{\text{pois}}(2.30)$	$\hat{\mathcal{Z}}(2.30)$	$\mathcal{Z}_{\text{pois}}(3.07)$	$\hat{\mathcal{Z}}(3.07)$
8	0.1	2.493×10^{-1}	$2.424(3) \times 10^{-1}$	1.407×10^{-1}	$1.48491(6) \times 10^{-1}$
12	0.8	1.155×10^{-2}	$1.145(3) \times 10^{-2}$	3.752×10^{-2}	$3.762(1) \times 10^{-2}$
20	1.6	2.676×10^{-2}	$2.583(2) \times 10^{-2}$	2.697×10^{-3}	$2.946(6) \times 10^{-3}$
30	3.4	4.372×10^{-3}	$4.12(2) \times 10^{-3}$	1.023×10^{-4}	$8.3(3) \times 10^{-4}$
50	5.5	1.169×10^{-4}	$1.20(4) \times 10^{-4}$	1.554×10^{-7}	$2.5(1.6) \times 10^{-7}$

for each volume. These are used to calculate the free energy density shown in Fig.11. We find by comparing Fig.2 that the flattening behaviors are not observed any longer.

§5. Summary

We have considered lattice field theory with a θ term, which suffers from the complex Boltzmann weight problem or the sign problem in numerical simulations. As an attempt at a different approach from the conventional procedure that employs the numerical Fourier transform of $P(Q)$, we have applied the MEM in order to reconstruct the partition function $\mathcal{Z}(\theta)$. We have employed the Gaussian $P(Q)$ as a test, since its Fourier transform is analytically performed. As a result, for the data without the flattening, the results of the

MEM analysis agree with those of the Fourier transform, while for those with the flattening, the MEM reproduces the images which are free from the flattening, and thus the flattening phenomenon is improved.

Comments are in order.

1. During the analysis, the condition $\mathcal{Z}(\theta) > 0$ in Eq. (3.14) is imposed as prior information I . This plays an important role in searching the maximal image in the case with the flattening. This condition could yield different results from those in the Fourier method where $\mathcal{Z}(\theta)$ could become negative due to the large errors.
2. It is important what default model is chosen for the analysis. A criterion for the choice is the magnitude of the errors of the averaged image, which are determined according to the probability. We have investigated various default models, and it is found that $\gamma = 3.4$ for $V = 30$ and $\gamma = 5.5$ for $V = 50$ are the best among those which we have investigated in the flattening case. The purpose of the present paper is to check the feasibility of application of the MEM to the issue of θ term and thus the value of γ in the case of Gaussian default is not chosen so extensively. There might be some better default models than those we have investigated here.
3. As volume increases, the flattening problem becomes severer, and higher precision of the computations becomes necessary. This is because more precise calculation is required to obtain the inverse of the covariance matrix of $P(Q)$ with increasing volume. In the case $V = 8$, for example, the Newton method works even with double precision. For $V = 50$, on the other hand, we need quadruple precision.
4. Since the flattening behavior is inherent in the Fourier procedure, quite independent of what model one deals with, we have used the Gaussian $P(Q)$ as a first attempt. The next issue is to apply the MEM to more realistic models such as the CP^{N-1} model and QCD and to investigate its feasibility. The MEM analysis might also be applicable to some other issues with the sign problem. It may be worthwhile to study whether it would work or not for issues such as lattice field theory with a finite density.

Acknowledgments

We are grateful to Prof.'s Shoichi Sasaki and Masayuki Asakawa for useful discussion about the MEM. This work is supported in part by Grants-in-Aid for Scientific Research (C)(2) of the Japan Society for the Promotion of Science (No. 15540249) and of the Ministry of Education Science, Sports and Culture (No.'s 13135213 and 13135217). Numerical calculations are partly performed on the computer at Computer and Network Center, Saga University.

Appendix A

— SVD and Newton method —

In order to obtain the maximal image of $\mathcal{Z}(\theta)$ for a fixed α , we must solve the following equation (See Eq. (3.16));

$$-\alpha \log \frac{\mathcal{Z}_n}{m_n} = \sum_{ij} K_{jn} C_{ij}^{-1} \delta P_j. \quad (\text{A.1})$$

For a latter convenience, we introduce a new parameter a_n

$$a_n \equiv \log \frac{\mathcal{Z}_n}{m_n}. \quad (\text{A.2})$$

We regard \mathcal{Z}_n and \bar{P}_j as N_θ and N_q dimensional vectors, respectively ($n = 1, 2, \dots, N_\theta$ and $j = 1, 2, \dots, N_q$). In our case, N_θ is $\mathcal{O}(10^1 \sim 10^2)$ and $N_q \sim \mathcal{O}(10^0)$. So it is non-trivial to find $\mathcal{Z}_n^{(\alpha)}$ satisfying Eq. (3.16). This task is considerably relieved by employing the SVD. The transpose of K , K^t , is decomposed to

$$(K^t)_{nj} = (U \Xi V^t)_{nj}, \quad (\text{A.3})$$

where U is an $N_\theta \times N_q$ matrix satisfying $U^t U = 1$, V an $N_q \times N_q$ orthogonal matrix and Ξ an $N_q \times N_q$ diagonal matrix $(\Xi)_{ij} = \xi_i \delta_{ij}$. Eigenvalues ξ_i , which are positive semi-definite, are called the singular values of K^t . They could be arranged by appropriate permutations such that $\xi_1 \geq \xi_2 \geq \dots \geq \xi_{N_s} > \xi_{N_{s+1}} = \dots = \xi_{N_q} = 0$, where

$$N_s = \text{rank}(K^t) \leq N_q. \quad (\text{A.4})$$

Following Bryan,¹³⁾ the first N_s column vectors of $U = (\mathbf{u}_1, \mathbf{u}_2, \dots, \mathbf{u}_{N_q})$ construct a basis in 'singular space', which is a subspace in N_θ dimensional space; the basis is $\{\mathbf{u}_1, \mathbf{u}_2, \dots, \mathbf{u}_{N_s}\}$ with $\mathbf{u}_i = (u_{1i}, u_{2i}, \dots, u_{N_\theta i})^t$. One can then place the vector \mathbf{a} in singular space

$$\mathbf{a} = \sum_{i=1}^{N_s} \lambda_i \mathbf{u}_i. \quad (\text{A.5})$$

Substituting Eq. (A.3) and Eq. (A.5) into Eq. (A.1), we find

$$-\alpha \sum_i \lambda_i U_{ni} = \sum_{i,j} (U \Xi V^t)_{ni} C_{ij}^{-1} \delta P_j. \quad (\text{A.6})$$

A use of $U^t U = 1$ yields

$$-\alpha \lambda_i = \sum_{j,l} (\Xi V^t)_{ij} C_{jl}^{-1} \delta P_l. \quad (\text{A.7})$$

To solve λ_i , the Newton method is employed. For each iteration, an increment $\delta\lambda$ is given by

$$\sum_k \left[-\alpha\delta_{ik} - \sum_{j,l,n} (\Xi V^t)_{ij} C_{jl}^{-1} K_{ln} \mathcal{Z}_n U_{nk} \right] \delta\lambda_k = \alpha\lambda_i + \sum_{j,l} (\Xi V^t)_{ij} C_{jl}^{-1} \delta P_l, \quad (\text{A.8})$$

or in the matrix notation

$$-X\delta\lambda = \alpha\lambda + Y\delta P, \quad (\text{A.9})$$

where λ and δP are N_q dimensional vectors, and X and Y are $N_s \times N_s$ and $N_s \times N_q$ matrices, respectively;

$$X \equiv \alpha\mathbf{1} + \Xi V^t C^{-1} K \mathcal{Z} U, \quad Y \equiv \Xi V^t C^{-1}. \quad (\text{A.10})$$

We then need to calculate the inverse matrix of X to obtain $\delta\lambda$. Note that $N_s = N_q$ holds for all the cases we have considered in the present paper.

Appendix B

— Derivation of Eqs. (3.23) and (3.28) —

1. Eq. (3.23) is derived as follows.

The probability $\text{prob}(\mathcal{Z}_n | P(Q), I, m)$ can be rewritten by use of the law of the total probability $\text{prob}(A) = \int dB \text{prob}(A, B)$ as follows;

$$\begin{aligned} \text{prob}(\mathcal{Z}_n | P(Q), I, m) &= \int d\alpha \text{prob}(\mathcal{Z}_n, \alpha | P(Q), I, m) \\ &= \int d\alpha \text{prob}(\mathcal{Z}_n | \alpha, P(Q), I, m) \text{prob}(\alpha | P(Q), I, m). \end{aligned} \quad (\text{B.1})$$

In the second line, the definition of the conditional probability was used.

Substituting Eq. (B.1) into Eq. (3.21), we obtain

$$\begin{aligned} \hat{\mathcal{Z}}_n &= \int [d\mathcal{Z}] \mathcal{Z}_n \int d\alpha \text{prob}(\mathcal{Z}_n | \alpha, P(Q), I, m) \text{prob}(\alpha | P(Q), I, m) \\ &= \int d\alpha \text{prob}(\alpha | P(Q), I, m) \int [d\mathcal{Z}] \mathcal{Z}_n \text{prob}(\mathcal{Z}_n | \alpha, P(Q), I, m) \\ &\simeq \int d\alpha \text{prob}(\alpha | P(Q), I, m) \mathcal{Z}_n^{(\alpha)}. \end{aligned} \quad (\text{B.2})$$

where we assumed that the probability $\text{prob}(\mathcal{Z}_n | \alpha, P(Q), I, m)$ has a sharp peak around $\mathcal{Z}_n^{(\alpha)}$. Utilizing the Bayes' theorem, the law of the total probability and the definition

of the conditional probability, the probability $\text{prob}(\alpha|P(Q), I, m)$ is rewritten as

$$\begin{aligned}
\text{prob}(\alpha|P(Q), I, m) &= \frac{\text{prob}(P(Q)|\alpha, I, m)\text{prob}(\alpha|I, m)}{\text{prob}(P(Q)|I, m)} \\
&= \frac{\text{prob}(\alpha|I, m)}{\text{prob}(P(Q)|I, m)} \int [d\mathcal{Z}] \text{prob}(P(Q), \mathcal{Z}_n|\alpha, I, m) \\
&= \frac{\text{prob}(\alpha|I, m)}{\text{prob}(P(Q)|I, m)} \int [d\mathcal{Z}] \text{prob}(P(Q)|\mathcal{Z}_n, \alpha, I, m) \\
&\quad \times \text{prob}(\mathcal{Z}_n|\alpha, I, m) \\
&\propto \text{prob}(\alpha|I, m) \int [d\mathcal{Z}] \frac{e^{W(\mathcal{Z})}}{X_L X_S(\alpha)}, \tag{B.3}
\end{aligned}$$

where Eq. (3.13) was used, and irrelevant factors such as $\text{prob}(P(Q)|I, m)$ were ignored. Expanding $W(\mathcal{Z})$ around $\{\mathcal{Z}^{(\alpha)}\}$ up to the second order, we can perform the Gaussian integration over configurations of $\{\mathcal{Z}\}$;

$$\begin{aligned}
&\text{prob}(\alpha|P(Q), I, m) \\
&\propto \text{prob}(\alpha|I, m) \int [d\mathcal{Z}] \frac{1}{X_L X_S(\alpha)} \exp \left\{ W(\mathcal{Z}^{(\alpha)}) + \frac{1}{2} \sum_{n,n'} \delta \mathcal{Z}_n \frac{\partial^2 W}{\partial \mathcal{Z}_n \partial \mathcal{Z}_{n'}} \delta \mathcal{Z}_{n'} \right\} \\
&\propto \text{prob}(\alpha|I, m) \exp \left\{ \frac{1}{2} \sum_k \log \frac{\alpha}{\alpha + \lambda_k} + W(\mathcal{Z}^{(\alpha)}) \right\} \\
&\equiv \text{prob}(\alpha|I, m) \exp \left\{ \Lambda(\alpha) + W(\mathcal{Z}^{(\alpha)}) \right\}, \tag{B.4}
\end{aligned}$$

where $\delta \mathcal{Z}_n \equiv \mathcal{Z}_n - \mathcal{Z}_n^{(\alpha)}$. Irrelevant constants were ignored as before. The values λ_k 's are eigenvalues of the real symmetric matrix in θ space defined in Eq. (3.24). The prior probability $\text{prob}(\alpha|I, m)$ is conventionally chosen to be either the Laplace' rule ($\text{prob}(\alpha|I, m) = \text{const}$) or the Jeffrey's rule ($\text{prob}(\alpha|I, m) = 1/\alpha$). Since the integral in Eq. (B.2) is insensitive to the choice of $\text{prob}(\alpha|I, m)$ as long as $\text{prob}(\alpha|I, m)$ has a sharp peak, we employ the Laplace's rule for simplicity.^{16),13)}

Substituting Eq. (B.4) into Eq. (B.2), we can obtain the equation of $\hat{\mathcal{Z}}_n$.

$$\hat{\mathcal{Z}}_n = \frac{1}{X_W} \int d\alpha \mathcal{Z}_n^{(\alpha)} \exp \left\{ \frac{1}{2} \sum_k \log \frac{\alpha}{\alpha + \lambda_k} + W(\mathcal{Z}^{(\alpha)}) \right\}. \tag{B.5}$$

2. Eq. (3.28) is derived as follows.

The uncertainty of the final output image $\hat{\mathcal{Z}}_n$ is calculated as follows.¹⁶⁾

$$\langle (\delta \hat{\mathcal{Z}}_n)^2 \rangle \equiv \int d\alpha \langle (\delta \mathcal{Z}_n^{(\alpha)})^2 \rangle \text{prob}(\alpha|P(Q), I, m), \tag{B.6}$$

where

$$\langle (\delta \mathcal{Z}^{(\alpha)})^2 \rangle \equiv \frac{\int [d\mathcal{Z}] \int_{\Theta} d\theta_n d\theta_{n'} \delta \mathcal{Z}_n \delta \mathcal{Z}_{n'} \text{prob}(\mathcal{Z}_m | P(Q), I, m, \alpha)}{\int [d\mathcal{Z}] \int_{\Theta} d\theta_n d\theta_{n'} \text{prob}(\mathcal{Z}_m | P(Q), I, m, \alpha)}. \quad (\text{B.7})$$

Using $\int [d\mathcal{Z}] \text{prob}(\mathcal{Z}_m | P(Q), I, m) \equiv 1$ and inserting Eq. (3.13), we obtain

$$\langle (\delta \mathcal{Z}^{(\alpha)})^2 \rangle = \frac{1}{\int_{\Theta} d\theta_n d\theta_{n'}} \int_{\Theta} d\theta_n d\theta_{n'} \int [d\mathcal{Z}] \delta \mathcal{Z}_n \delta \mathcal{Z}_{n'} \frac{e^{W(\mathcal{Z})}}{X_L X_S(\alpha)}. \quad (\text{B.8})$$

When $e^{W(\mathcal{Z})}$ is expanded around $\{\mathcal{Z}^{(\alpha)}\}$ up to the second order and the integral over \mathcal{Z}_n is performed, Eq. (3.28) is derived as

$$\begin{aligned} \langle (\delta \mathcal{Z}^{(\alpha)})^2 \rangle &= \frac{1}{\int_{\Theta} d\theta_n d\theta_{n'}} \int_{\Theta} d\theta_n d\theta_{n'} \int [d\mathcal{Z}] \delta \mathcal{Z}_n \delta \mathcal{Z}_{n'} \frac{1}{X_L X_S(\alpha)} \\ &\quad \times \exp \left\{ W(\mathcal{Z}^{(\alpha)}) + \frac{1}{2} \sum_{n,n'} \delta \mathcal{Z}_n \frac{\partial^2 W}{\partial \mathcal{Z}_n \partial \mathcal{Z}_{n'}} \delta \mathcal{Z}_{n'} \right\} \\ &\simeq -\frac{1}{\int_{\Theta} d\theta_n d\theta_{n'}} \int_{\Theta} d\theta_n d\theta_{n'} \left(\frac{\partial^2 W}{\partial \mathcal{Z}_n \partial \mathcal{Z}_{n'}} \Big|_{\mathcal{Z}=\mathcal{Z}^{(\alpha)}} \right)^{-1}. \end{aligned} \quad (\text{B.9})$$

Appendix C

— Uniqueness of a maximum of W —

Following Asakawa et.al.,¹⁶⁾ let us check that a maximum of W uniquely exists for $\alpha \neq 0 (> 0)$. In our case the kernel is given by that of the Fourier transform. The curvature of W is given by

$$\frac{\partial^2 W}{\partial \mathcal{Z}_m \partial \mathcal{Z}_n} = -\alpha \delta_{mn} \frac{1}{\mathcal{Z}_n} - \sum_{ij} K_{im} C_{ij}^{-1} K_{jn}. \quad (\text{C.1})$$

Introducing any N_{θ} dimensional real vector $\mathbf{y} (\neq 0)$, let us calculate

$$\sum_{mn} y_m \frac{\partial^2 W}{\partial \mathcal{Z}_m \partial \mathcal{Z}_n} y_n = \sum_{mn} y_m \left[-\alpha \delta_{mn} \frac{1}{\mathcal{Z}_n} - \sum_{ij} K_{im} C_{ij}^{-1} K_{jn} \right] y_n. \quad (\text{C.2})$$

1. $\alpha = 0$ case

When $\alpha = 0$, Eq. (C.2) becomes

$$\sum_{mn} y_m \frac{\partial^2 W}{\partial \mathcal{Z}_m \partial \mathcal{Z}_n} y_n = - \sum_{mn} y_m \sum_{ij} K_{im} C_{ij}^{-1} K_{jn} y_n. \quad (\text{C.3})$$

Since the covariance matrix C is symmetric, C is diagonalized by an $N_q \times N_q$ orthogonal matrix R as

$$R^t C R = \bar{\sigma}^2.$$

Also a defining $N_q \times N_\theta$ matrix

$$\tilde{K} \equiv R^t K,$$

and an N_q dimensional real vector

$$\tilde{\mathbf{y}} \equiv \tilde{K}\mathbf{y}, \quad (\text{C.4})$$

Eq. (C.3) becomes

$$\sum_{mn} y_m \frac{\partial^2 W}{\partial \mathcal{Z}_m \partial \mathcal{Z}_n} y_n = - \sum_i \frac{\tilde{y}_i^2}{\bar{\sigma}_i^2} \leq 0. \quad (\text{C.5})$$

This could be vanishing only for $\tilde{\mathbf{y}} = 0$, and this realizes for non-trivial vectors \mathbf{y} , because Eq. (C.4) tells that the dimension of solution vector space is

$$N_\theta - \text{rank } \tilde{K} \geq N_\theta - N_q > 0.$$

In the $\alpha = 0$ case, therefore, maxima of W are degenerated.

2. $\alpha \neq 0$ case

For $\alpha \neq 0$, Eq. (C.2) becomes

$$\sum_{mn} y_m \frac{\partial^2 W}{\partial \mathcal{Z}_m \partial \mathcal{Z}_n} y_n = -\alpha \sum_n \frac{y_n^2}{\mathcal{Z}_n} - \sum_i \frac{\tilde{y}_i^2}{\bar{\sigma}_i^2}. \quad (\text{C.6})$$

Since $\mathcal{Z}_n > 0$, the curvature of W becomes negative definite

$$\sum_{nm} y_m \frac{\partial^2 W}{\partial \mathcal{Z}_m \partial \mathcal{Z}_n} y_n < 0.$$

Therefore the entropy term is essential to the uniqueness of the maximum.

Appendix D

— Comparison with the Fourier method —

In the the case of no flattening, we show that the analysis in the Newton method leads to the same result as that obtained by the Fourier method. This holds for $\alpha = 0$ and $\alpha \neq 0$ (but small $\alpha > 0$). Note that in the Fourier method,

$$\bar{P} = K\mathcal{Z} \quad (\text{D.1})$$

is successfully inverted in the case without the flattening. This is because $P(Q)$ is rapidly decreasing function, and $\mathcal{Z}(\theta)$, which is given by the Fourier transform, is smooth enough that one can neglect the contribution from higher Q .

1. $\alpha = 0$ case

Let us first consider the $\alpha = 0$ case. For $\alpha = 0$, Eq. (A.9) reduces to

$$-X_0\delta\lambda = Y\delta P, \quad (\text{D.2})$$

where

$$X_0 \equiv \Xi V^t C^{-1} K Z U. \quad (\text{D.3})$$

When X_0 is regular, increment $\delta\lambda$ becomes

$$\delta\lambda = -X_0^{-1}Y\delta P. \quad (\text{D.4})$$

When the iterations converge $\delta\lambda = 0$ in the Newton method, we find

$$X_0^{-1}Y\delta P = 0. \quad (\text{D.5})$$

Since the $N_q \times N_q$ matrix $X_0^{-1}Y$ is regular (this is checked numerically),

$$\delta P = K\mathcal{Z} - \bar{P} = 0 \quad (\text{D.6})$$

is a unique solution.

Eq. (D.6) gives N_q equations

$$\sum_{n=1}^{N_\theta} K_{in} m_n \exp\left(\sum_{j=1}^{N_q} U_{nj} \lambda_j\right) = \bar{P}_i \quad (i = 1, \dots, N_q). \quad (\text{D.7})$$

Thus one obtains a unique solution for $\lambda_i (i = 1, \dots, N_q)$ for a given default m_n . This turns out to give \mathcal{Z}_n , which is equivalent to that in the Fourier method.

2. $\alpha \neq 0$ case (small α)

When $\alpha \neq 0$, we use Eq. (A.9) in the Newton method. For small α , this is approximated by

$$X\delta\lambda = -Y\delta P. \quad (\text{D.8})$$

By using the regularity of X , $\delta\lambda$ is given by

$$\delta\lambda = -X^{-1}Y\delta P. \quad (\text{D.9})$$

For a converging point in the iterations, the regularity of $X^{-1}Y$ allows

$$\delta P = 0, \quad (\text{D.10})$$

which is the same as Eq. (D.6). Therefore we also obtain a unique solution.

We thus find for $\alpha = 0$ and/or for small values of α that the Newton method leads to the same result $\mathcal{Z}_n^{(\alpha)}$ as the one obtained by the Fourier method. Moreover, if the probability $\text{prob}(\alpha|P(Q), I, m)$ dominates at $\alpha \approx 0$, then the averaged image $\hat{\mathcal{Z}}_n$ is also in good agreement with the Fourier method. Actually this is the case for the cases without the flattening, as discussed in section 4.1.

References

- 1) G. 't Hooft, Nucl. Phys. **B190** [FS3] (1981), 455.
- 2) J. L. Cardy and E. Rabinovici, Nucl. Phys. **B205** [FS5] (1982), 1.
J. L. Cardy, Nucl. Phys. **B205** [FS5] (1982), 17.
- 3) N. Seiberg, Phys. Rev. Lett. **53** (1984), 637.
- 4) A. S. Hassan, M. Imachi, N. Tsuzuki and H. Yoneyama, Prog. Theor. Phys. **95** (1995), 175.
- 5) M. Imachi, S. Kanou and H. Yoneyama, Prog. Theor. Phys. **102** (1999), 653 .
- 6) G. Bhanot, E. Rabinovici, N. Seiberg and P. Woit, Nucl. Phys. **B230** [FS10] (1984), 291.
- 7) U. -J. Wiese, Nucl. Phys. **B318** (1989), 153.
W. Bietenholz, A. Pochinsky and U. -J. Wiese, Phys. Rev. Lett. **75** (1995), 4524.
- 8) J. C. Plefka and S. Samuel, Phys. Rev. **D56** (1997), 44.
- 9) R. Burkhalter, M. Imachi, Y. Shinno and H. Yoneyama, Prog. Theor. Phys. **106** (2001), 613.
- 10) S. Olejnik and G. Schierholz, Nucl. Phys. **B** (Proc.Suppl) **34** (1994), 709.
- 11) V. Azcoiti, G. Di Carlo, A. Galante and V. Laliena, Phys. Rev. Lett. **89** (2002), 141601.

V. Azcoiti, G. Di Carlo, A. Galante and V. Laliena, hep-lat/0305022.

- 12) J. Ambjorn, K. N. Anagnostopoulos, J. Nishimura and J. J. M. Verbaarschot, J. High Energy Phys. **0210** (2002), 062.
- 13) R. K. Bryan, Eur. Biophys. J. **18** (1990), 165.
- 14) R. N. Silver, D. S. Sivia and J. E. Gubernatis, Phys. Rev. **B41** (1990), 2380.
- 15) J. E. Gubernatis, M. Jarrell, R. N. Silver and D. S. Sivia, Phys. Rev. **B44** (1991), 6011.
- 16) M. Asakawa, T. Hatsuda and Y. Nakahara, Prog. Part. Nucl. Phys. **46** (2001), 459.
- 17) CP-PACS Collaborations, T. Yamazaki et. al., Phys. Rev. **D65** (2002), 014501.
- 18) S. Sasaki, nucl-th/0305014.
- 19) T. Yamazaki and N. Ishizuka, Phys. Rev. **D67** (2003), 077503.
- 20) M. Karliner, S. R. Sharpe and Y. F. Chang, Nucl. Phys. **B302** (1988), 204.